RADIOLOGICAL AND LEACHING ASSESSMENT OF AN ETTRINGITE-BASED MORTAR FROM LADLE SLAG AND PHOSPHOGYPSUM

Katrijn GIJBELS[a*], Hoang NGUYEN[b], Paivo KINNUNEN[b], Pieter SAMYN[c], Wouter SCHROEYERS[a], Yiannis PONTIKES[d], Sonja SCHREURS[a], Mirja ILLIKAINEN[b]

[a] Hasselt University, CMK, Nuclear Technological Centre, Agoralaan, Gebouw H, 3590 Diepenbeek, Belgium

[b] Fibre and Particle Engineering Research Unit, University of Oulu, Pentti Kaiteran katu 1, 90014 Oulu, Finland

[c] Hasselt University, IMO, Applied and Analytical Chemistry, Agoralaan, Gebouw D, 3590 Diepenbeek, Belgium

[d] KU Leuven, Department of Materials Engineering, Kasteelpark Arenberg 44, 3001 Leuven, Belgium

* Corresponding author: Katrijn GIJBELS

katrijn.gijbels@uhasselt.be, hoang.nguyen@oulu.fi, paivo.kinnunen@oulu.fi, pieter.samyn@uhasselt.be, wouter.schroeyers@uhasselt.be, yiannis.pontikes@kuleuven.be, sonja.schreurs@uhasselt.be, mirja.illikainen@oulu.fi

Declarations of interest: none

24 **Highlights:**

25 - Ettringite-based mortars were produced from ladle slag and phosphogypsum

26 - The mortars comply with the legislation on naturally occurring radionuclides in

27 building materials

28 - The radon emanation was mainly dependent on the microporosity when using Polish

29 phosphogypsum

30 - Specific surface areas were 20-30 times lower than conventional cement

31 - The mortars show a high degree of immobilization for contaminants contained in

32 phosphogypsum

33

34 **Abstract**

35 In this investigation, ettringite-based mortars were synthesized from ladle slag (LS) and

36 phosphogypsum (PG), promoting the concept of a circular economy. However, the reuse of

37 naturally occurring radioactive materials (NORM), such as PG, requires radiological

38 investigation. Also, the immobilization degree for contaminants contained in PG should be

39 evaluated. The former was investigated using gamma spectroscopy and radon

40 exhalation/emanation tests, while the latter was assessed using an up-flow percolation

41 column test according to the CEN/TS 16637-3. The produced mortars comply with current

42 legislation on naturally occurring radionuclides (NOR) in building materials, proving that they

43 can be safely used for building purposes. The radon emanation decreased upon increasing

44 the Polish PG content, which was mainly determined by the microporosity. The specific

45 surface areas were 20-30 times lower than conventional cement, and the immobilization

46 degree for contaminants was generally high (> 90%). This investigation demonstrates high

47 potential for PG reuse in ettringite-based mortars.

48

49 **Keywords**

50 Ladle slag, phosphogypsum, ettringite, naturally occurring radionuclides, leaching

51

1. Introduction

53 In the development of a more sustainable construction industry, many research efforts are

54 focused on the partial or even total replacement of Ordinary Portland Cement (OPC) content

55 with by-products [1], for example, slags [2,3]. One such by-product is ladle slag (LS) from the

56 steel-making process [4,5]. Unlike other slags, LS has gained much less attention due to its

57 crystallinity and free CaO content. About 80% of LS generated in Europe is landfilled or

58 stored [5], which amounts to roughly 1.5-1.9 million tons annually. However, the feasibility of

59 LS for the production of cementitious materials has been advocated in the literature, e.g. as a

60 sole precursor in alkali-activated pastes [6], mortars [7] and composites [8], with promising

61 mechanical properties.

62 LS can also effectively be used for the synthesis of ettringite-based binders from its hydration

63 with gypsum and water [9–11]. Generally, ettringite-based binders show rapid strength gain

64 and are compatible with conventional cementitious matrices [12]. Since alkali silicates and

65 hydroxides cannot be sourced naturally, their production involves costs and energy usage,

66 significantly contributing to the environmental footprint of alkali-activated binders [13].

67 Therefore, ettringite-based binders, which do not require alkali activation, are very promising

68 materials from both an economical and sustainability perspective. Further, the abundance of

69 various types of gypsum waste shows the potential for their use as a calcium sulfate source,

70 making this practice even more environmentally and economically beneficial [14].

71 From a chemical point of view, phosphogypsum (PG) - a by-product in the phosphate

72 fertilizer industry - is an excellent potential calcium sulfate source. However, PG can be

73 classified as a naturally occurring radioactive material (NORM) due to elevated

74 concentrations of radium [15,16]. PG also contains impurities such as phosphates, fluorides,

75 heavy metals and other trace elements [16], placing many restrictions on its reuse. The

76   impurity composition is greatly dependent on the origin of the phosphate rock used and to a

77   lesser extent on differences in process plant operation and the PG's age. PG is currently

78   being added to stacks at an annual rate of about 100-280 million tons worldwide [16], and

79   approximately 3 billion tons have already been stacked in well over 50 countries [17].

80   Furthermore, the production of PG is expected to increase in the coming decades as a

81   consequence of rising food demand. Basic and applied research is necessary to widen its

82   field of application, provided that such practice will not cause additional risks to the public or

83   the environment.

84   The reuse of NORM in building materials requires radiological characterization because it

85   can enhance both the external and internal dose rate for residents, induced by gamma

86   radiation and the inhalation of radon, respectively [18–21]. In this respect, indexes are

87   commonly used as a screening aid in the decision whether or not a NORM can be used for

88   building purposes. In other words, (partially) NORM-based building materials may not exceed

89   levels stated in the index used. Current Chinese and Russian legislation is based on the

90   calculation of the radium equivalent index (Ra_{eq}) [22,23]. In European countries, the gamma

91   dose rate imposed by building materials is regulated by the European Basic Safety

92   Standards (EU-BSS), which operate on the calculation of the activity concentration index

93   (ACI) [24]. However, there exist no specific regulations concerning radon release from

94   building materials, although this should be kept as low as possible as this radionuclide is

95   classified by the International Agency for Research on Cancer (IARC) as a Group 1 human

96   carcinogen [25] in the case of long term exposure. Radon can be released from the solid

97   matrix by recoil when radium decays (referred to as emanation) and leaves the building

98   material through the pore network (referred to as exhalation) by diffusion or advective flow

99   [26]. There exist three naturally occurring radon isotopes (i.e., [219]Rn, [220]Rn and [222]Rn), but

100   only [222]Rn is generally of significance from the radiation protection point of view [27] and

101   hence is further considered in this study.

102   Upon reuse, the presence of impurities contained in the PG may not lead to secondary

103   pollution. Ettringite ($(CaO)_6(Al_2O_3)(SO_3)_3.32H_2O$, or in cement chemists' notation $C_6A\bar{S}_3H_{32}$),

104   however, can incorporate a number of ions in its crystal structure [28–30] and therefore act

105   as an immobilization agent. The effectiveness of such immobilization can be evaluated by a

106   leaching assessment. In this respect, a column test provides reliable field-correlated

107   information [31]. On the European level, the CEN/TC 351 [32] provides valuable guidance for

108   testing the release of dangerous substances from construction products into soil, surface

109   water and ground water, including the column leaching protocol CEN/TS 16637-3 [33], which

110   is applied in this study.

111   In this investigation, ettringite-based mortars from LS and PG are developed for use as an

112   alternative binder for OPC in the building industry. Since PG is considered as NORM, the

113   radiological impact (i.e., gamma dose rate and the release of radon) is evaluated. The

114   microstructural features are evaluated using scanning electron microscopy (SEM) coupled

115   with X-ray energy dispersive spectroscopy (EDS). The immobilization of impurities is

116   assessed by means of an up-flow percolation leaching test according to the CEN/TS 16637-

117   3. Nitrogen adsorption/desorption was applied to investigate the porosity features. This study

118   complements a parallel study wherein the hydration, mineralogy and compressive strength

119   were investigated for the same binder mixtures [34].

120

121   **2. Materials and methods**

122   **2.1 Materials**

123   The LS was provided by SSAB Europe Oy (Raahe, Finland) after exposure to natural

124   conditions at its cooling pit. The free CaO content was measured following EN 450-1 [35] and

125   found to be zero. The LS was ball-milled (TPR-D-950-V-FU-EH, Germatec Germany) to

126   obtain a d_{50} value of 10 µm. As calcium sulfate source, 3 different products were used

127   (hereafter referred to as G1, G2 and G3, respectively). G1 constituted synthetic

128 $CaSO_4.2H_2O$, supplied by VWR (product code 22451.360). G2 was PG provided by Yara Oy

129 (Finland). G3 was PG collected from a plant in Gdansk (Poland) and was milled and

130 homogenized by the International Atomic Energy Agency (IAEA) (reference material n° 434)

131 [36]. To remove excess moisture, G2 was dried at 333.15 K in a laboratory oven for 24 h.

132 The particle size distribution of LS, G1, G2 and G3 is presented in [34]. No additional milling

133 was performed for G2 and its unimodal particle size distribution ranged from 0.1 μm to 324

134 μm. G1 and G3 were used as received with unimodal particle size distributions ranging from

135 0.2 μm to 66 μm and from 0.2 μm to 24 μm, respectively. The d_{50} value for LS, G1, G2 and

136 G3 was 10 μm, 12 μm, 66 μm and 7 μm, respectively. X-ray fluorescence analysis (XRF)

137 (Philips PW 1830) was applied to obtain the chemical composition of the LS and G2. The

138 matrix composition of G3 was provided by the IAEA and was: 96 wt% $CaSO_4.2H_2O$, 1-2 wt%

139 P_2O_5, 1.2 wt% F^-, 1 wt% SiO_2 and 0.2 wt% Al_2O_3 [36]. The chemical composition of the

140 materials is summarized in Table 1.

141   **Table 1**: Chemical composition (in wt%) of LS, G1, G2 and G3

	LS	G1	G2	G3
CaO (C)	51.1	41.2	45.9	39.5
SiO_2 (S)	14.1	-	0.2	1.0
Al_2O_3 (A)	24.6	-	0.3	0.2
Fe_2O_3 (F)	0.5	-	-	-
SrO	$32.2\ 10^{-3}$	-	0.8	-
MgO	3.8	-	0.2	-
SO_3^- ($\bar{S}$)	0.4	58.8	51.4	56.5
TiO_2	4.2	-	-	-
CeO_2	-	-	0.3	-
P_2O_5	-	-	0.6	1.5
F^-	-	-	-	1.2

MnO	1.1	-	-	-
Others	0.2	-	0.3	0.1

142

143 A Bruker D2 PHASER was operated at 30 kV and 10 mA to investigate the mineralogy of the

144 LS, G1, G2 and G3, which is summarized in Table 2. A counting time of 0.3 s per step with a

145 step size of 0.02° was used for examinations over the range from 5° to 70° 2θ in continuous

146 PSD fast mode. Prior to the measurement, the powders were mixed with 10 wt% of

147 analytical-grade crystalline ZnO (99.9% purity, Merck) as an internal standard. The samples

148 were prepared using the back loading technique. During the measurement, an anti-scatter

149 slit was positioned 1 mm above the samples and they were rotated at 15 rpm. Qualitative

150 analysis was performed with EVA V.3.1 (Bruker AXS). MAUD (Material Analysis Using

151 Diffraction) [37] was used for quantitative analysis based on the Rietveld method [38]. The

152 phase contents were recalculated based on the known initial ZnO content.

153 $\qquad$ **Table 2**: Mineralogy (in wt%) of LS, G1, G2 and G3

	LS	G1	G2	G3
Calcio-olivine ($\gamma-C_2S$)	21.0	-	-	-
Tricalcium-aluminate (C_3A)	2.3	-	-	-
Mayenite ($C_{12}A_7$)	21.9	-	-	-
Periclase (MgO)	2.1	-	-	-
Perovskite (CaTiO$_3$)	1.3	-	-	-
Calcium aluminum magnesium silicate (Ca$_{20}$Al$_{26}$Mg$_3$Si$_3$O$_{68}$)	47.3	-	-	-
Gypsum ($C\bar{S}.2H$)	-	96.8	93.6	33.2
Bassanite ($C\bar{S}.0.5H$)	-	-	6.4	27.1
Anhydrite ($C\bar{S}$)	-	3.2	-	32.1

Amorphous	4.0	-	-	7.6

154

2.2 Gamma spectroscopy

156 About 300 g of homogenized LS and G2 were stored in an airtight polystyrene cylindrical

157 container of 250 cm³ with metal screwcap for 30 days to attain radioactive equilibrium of

158 ^{226}Ra and ^{228}Th and their progenies. G1 is assumed to contain a negligible amount of

159 naturally occurring radionuclides (NOR) and the NOR content of G3 was provided by the

160 IAEA. The measurements were performed using a High-Purity Germanium (HPGe) detector

161 (Mirion Technologies, Canberra, model BE5075-7500SI), coupled with a Lynx multi-channel

162 analyzer. Details of the HPGe detector and technique have been given elsewhere [27]. The

163 ^{234}Th activity concentration was estimated from the 63.3 keV (3.75%) gamma peak. The

164 ^{226}Ra activity concentration (A_{Ra-226}) was estimated from the 609.3 keV (45.5%), 1120.3 keV

165 (14.9%), 1729.6 keV (2.8%) and 1764.5 keV (15.3%) gamma peaks from ^{214}Bi and from the

166 351.9 keV (35.6%) gamma peak from ^{214}Pb. The ^{210}Pb activity concentration was estimated

167 from its 46.5 keV (4.2%) gamma peak. The ^{232}Th activity concentration (A_{Th-232}) was

168 estimated from the 911.2 (26.2%) gamma peak from ^{228}Ac and from the 238.6 (43.6%)

169 gamma peak from ^{212}Pb. The activity concentration of ^{208}Tl was estimated from the 583.2 keV

170 (85.0%) gamma peak and was corrected for branching [39]. The ^{40}K activity concentration

171 (A_{K-40}) was estimated using the 1460.8 keV (10.6%) gamma peak from ^{40}K itself. The decay

172 data are taken from the DDEP (Decay Data Evaluation Project) [40]. The ^{235}U decay chain is

173 not considered in this study because of its low abundancy.

174

2.3 Sample synthesis

176 By varying the ratios of LS, G1, G2 and G3 in the binder, a total of 7 mortar samples (M0-

177 M6) were prepared. The binder mixtures are shown in Table 3. As set retarder, a 0.5 wt%

178 citric acid solution was prepared by dissolving citric acid (supplied by Tokyo Chemical

179   Industry Co., Ltd., Japan, product code C1949) in distilled water (ASTM type II) using

180   magnetic stirring at a speed of 250 rpm for 30 min at room temperature. The mortar samples

181   were prepared according to EN 196-6 [41] using CEN standard sand (DIN EN 196-1) with a

182   sand-to-binder ratio (S/B) of 3. The liquid-to-binder ratio (L/B) was established at 0.45 based

183   on previous experimental work [9]. After mixing, the mortars were cast in silicon cubic molds

184   of 3.5 cm × 3.5 cm × 3.5 cm, whereafter the molds were stored in sealed plastic bags to

185   avoid the evaporation of water. The samples were demolded after 24 h and further cured for

186   28 days in a water bath at room temperature. After 28 days of curing, samples were air-dried

187   at room temperature for 2 days, whereafter they were dried in a laboratory oven at 313.15 K

188   for 2-3 days until a constant weight was achieved. Prior to testing, the mortar samples were

189   cooled down to room temperature in a desiccator. For SEM/EDS, paste samples were

190   prepared with a L/B of 0.45. After mixing, the casting and curing regimes were similar as for

191   the mortars. After their curing period, the hydration of the pastes was stopped by solvent

192   exchange using isopropanol.

193   **Table 3**: Binder mixtures (in wt%)

	LS	G1	G2	G3
M0	70	30	0	0
M1	70	20	10	0
M2	70	10	20	0
M3	70	0	30	0
M4	70	20	0	10
M5	70	10	0	20
M6	70	0	0	30

194

195   **2.4 Calculation of indexes for screening of gamma dose rate**

196   Based on the binder mixtures presented in Table 3, the Ra_{eq} [22,23] and the ACI [24] were

197   calculated (Eq. 1 and Eq. 2, respectively) for both paste and mortar samples allowing a

198   conservative screening. For mortar samples, the mass of the standard sand was included

199   and it was assumed that there are no NOR present in the standard sand.

200     $$Ra_{eq} = A_{Ra-226} + 1.43 \, A_{Th-232} + 0.077 \, A_{K-40} \quad (Eq.\, 1)$$

201     $$ACI = \frac{A_{Ra-226}}{300 \, Bq/kg} + \frac{A_{Th-232}}{200 \, Bq/kg} + \frac{A_{K-40}}{3000 \, Bq/kg} \quad (Eq.\, 2)$$

202   A Ra_{eq} value lower than 370 Bq/kg suggests an indoor external gamma exposure below 1.5

203   mSv/y [42], while an ACI below 1 indicates a possible indoor external gamma exposure

204   below 1 mSv/y [24]. In case the Ra_{eq} value of a given material exceeds the reference level of

205   370 Bq/kg, the potential applications of such a material are categorized as follows: (1) $Ra_{eq}<$

206   370 Bq/kg: for building residential houses; (2) 370 Bq/kg < Ra_{eq} < 740 Bq/kg: for industrial

207   use; (3) 740 Bq/kg < Ra_{eq} < 2200 Bq/kg: for roads and railways; (4) 2200 Bq/kg < Ra_{eq} <

208   3700 Bq/kg: for landfilling; and (5) Ra_{eq} > 3700 Bq/kg: forbidden to use for any construction

209   [43]. The ACI is applied for building materials (e.g. concrete, ceramics, bricks or gypsum

210   board) or their constituents if they are also building materials. In case those constituents are

211   separately assessed, an appropriate partitioning factor needs to be applied. If the ACI

212   exceeds the value of 1, an elaborated dose calculation needs to be executed to evaluate

213   whether their use in building applications is justified [44,45].

214

215   **2.5 Radon exhalation and emanation**

216   The radon exhalation (Ex_{Rn}) (in Bq/(kg*h)) of the mortars was determined with a SARAD

217   RadonScout PMT radon monitor (Lucas cell, ZnS scintillator with an active volume of 0.3

218   dm³) by enclosing the sample in a plexiglass accumulation chamber of 2 dm³. The

219   measurement of the radon concentration (C) (in Bq/m³) was performed as previously

220   described in [27]. The accumulation period ranged from 3-4 days and the measurements

221   were executed in triplicate under laboratory conditions (temperature 293.15 ± 2 K, relative

222   humidity about 50%). Since only [222]Rn is considered, C was calculated from the data

223   obtained in the interval from 2.5-4.0 h after the pump was stopped. The Ex_{Rn} was calculated

224   by the slope of the initial linear region of C, according to Eq. 3 [46]:

225
$$Ex_{Rn} = \left[\frac{C\,V}{m\,t}\right]\left[\frac{\lambda^*\,t}{1 - e^{-\lambda^*\,t}}\right]\ \ (Eq.\,3)$$

226   where V is the volume of the accumulation chamber (in m³), m is the mass of the mortar

227   sample (in kg), t is the time (in h) and λ^* (/h) is the effective [222]Rn decay constant

228   (determined as explained in [27]). The emanation factor Em_{Rn} (in %) is calculated using the

229   A_{Ra-226} of the mortar samples from the 30th day with Eq. 4 [47]:

230
$$Em_{Rn} = \frac{A_{Rn}^{out}}{A_{Ra}^{in}}\ 100\ \ (Eq.\,4)$$

231   where A_{Rn}^{out} is the calculated radon activity in the chamber after accumulation (in Bq) and A_{Ra}^{in}

232   is A_{Ra-226} (in Bq).

233

234   **2.6 Microstructural analysis**

235   The microstructure of paste samples was evaluated through SEM using a Zeiss Ultra Plus

236   instrument with a 15 kV accelerator voltage and a working distance of 7-8.5 mm. Prior to

237   evaluation, the pastes were vacuum-impregnated with epoxy resin, whereafter they were

238   polished using diamond discs of 220-1 μm at 150 rpm with ethanol as lubricant. The pastes

239   were observed using backscattered electrons (BSE). EDS was used to determine the

240   chemical compositions.

241

242   **2.7 Leaching assessment**

243 The leaching of mortar samples was assessed with an up-flow percolation test on granular

244 material, according to CEN/TS 16637-3 [33]. The sample preparation, measurement

245 circumstances, experimental set-up and the execution of the leaching test were the same as

246 in [48]. Distilled water (ASTM type II) was chosen as leachant solution. After a saturation

247 period of 20 h, 7 eluate fractions were collected at predefined intervals (0.10 ± 0.02 l/kg, 0.10

248 ± 0.02 l/kg, 0.30 ± 0.05 l/kg, 0.50 ± 0.05 l/kg, 1.00 ± 0.05 l/kg, 3.0 ± 0.1 l/kg, 5.0 ± 0.2 l/kg)

249 until a cumulative liquid-over-solid ratio (L/S) of 10.0 ± 0.5 l/kg was obtained. Immediately

250 after collection, the pH (HI2211 pH/ORP Meter, HANNA Instruments) and conductivity

251 (Konduktometer CG 858, Schott Geräte) of each eluate fraction were measured. During the

252 leaching test, the bottles for collection of the eluates were covered with plastic foil in order to

253 minimize carbonation. The eluate fractions were analyzed by inductively coupled plasma

254 optical emission spectrometry (ICP-OES, Perkin Elmer Optima 8300, RSD < 2%) for analysis

255 of Al, Ca, Ce, Fe, Mg, Mn, P, S, Si, Sr and Ti and ion-chromatography (IC, Dionex DX120)

256 for analysis of F. For IC, an analytical column (IonPac AS14A) equipped with a conductivity

257 detector was used, the pH of the eluates was buffered using 1 mM $NaHCO_3$ (supplied by

258 Merck) and 8 mM Na_2CO_3 (supplied by Merck).

259

260 **2.8 Nitrogen adsorption/desorption**

261 Nitrogen adsorption/desorption tests were carried out by a TRISTAR 3000 Micromeritics

262 device at 76.95 K. Prior to measurements, mortar samples were degassed using the flowing

263 degas process at 312.95 K under nitrogen flow for 12 h, with an input relative pressure of 2 ×

264 10^5 Pa. The specific surface area was derived from the nitrogen adsorption data over the

265 P/P_0 range of 0.05-0.30 (where P is the partial vapor pressure of the adsorbate gas in

266 equilibrium and P_0 is the saturated pressure of the adsorbate gas at 76.95 K) by the BET

267 (Brunauer, Emmett and Teller) method [49]. The Barrett-Joyner-Halenda (BJH) interpretation

268 was used to evaluate the mesopore size distribution and cumulative mesopore volume from

269   the adsorption isotherm [50]. The T-plot analysis method [51] was applied for determination

270   of the micropore volume and micropore specific surface area from the adsorption data.

271

272   **3. Results and discussion**

273   **3.1 Gamma spectroscopy**

274   The activity concentrations of the NOR are summarized in Fig. 1. The NOR content of G1 is

275   assumed to be negligible. Secular equilibrium between radium and progeny was established

276   for both the ^{238}U (^{226}Ra) and ^{232}Th (^{228}Ra) decay chains, as the activity concentration ratios

277   ^{214}Pb/^{214}Bi and ^{228}Ac/^{212}Pb ranged from 1.01 to 1.04 and 0.96 to 0.98, respectively [39]. World

278   average concentrations of ^{226}Ra, ^{232}Th and ^{40}K in the earth's crust are 40 Bq/kg, 40 Bq/kg

279   and 400 Bq/kg, respectively [52]. When comparing those values with the ones presented in

280   Fig.1, it is concluded that only G3 contains enhanced levels of NOR (more particularly ^{226}Ra

281   and progeny) as a consequence of its industrial processing [53]. G2 is characterized by a

282   very low natural radioactivity compared to the overall average in 12 EU member states

283   corresponding to 381 Bq/kg ^{226}Ra, 22 Bq/kg ^{232}Th and 71 Bq/kg ^{40}K in PG [21], which is

284   promising from the valorization point of view. For the LS, the NOR from the ^{238}U decay chain

285   were the most abundant compared to those from the ^{232}Th decay chain, while the opposite is

286   observed for G2. This is a consequence of the terrestrial radionuclides from natural origin

287   present in the mineral ore that has been processed. The presence and concentration of ^{232}Th

288   in G2 are uncertain as ^{232}Th cannot be measured directly by gamma spectroscopy, though its

289   concentration was equated with the ^{228}Ra activity concentration in this study. However, one

290   should keep in mind that the latter is only valid if there is secular equilibrium in the upper part

291   of the ^{232}Th decay chain. The measured intensities of ^{40}K and ^{234}Th were below the detection

292   limit for G2. This was also the case for ^{40}K, ^{228}Ac, ^{212}Pb and ^{208}Tl for G3. Pb becomes volatile

293   in high-temperature environments, which explains the reduced activity concentration of ^{210}Pb

294   for LS that is generated by high-temperature processing.
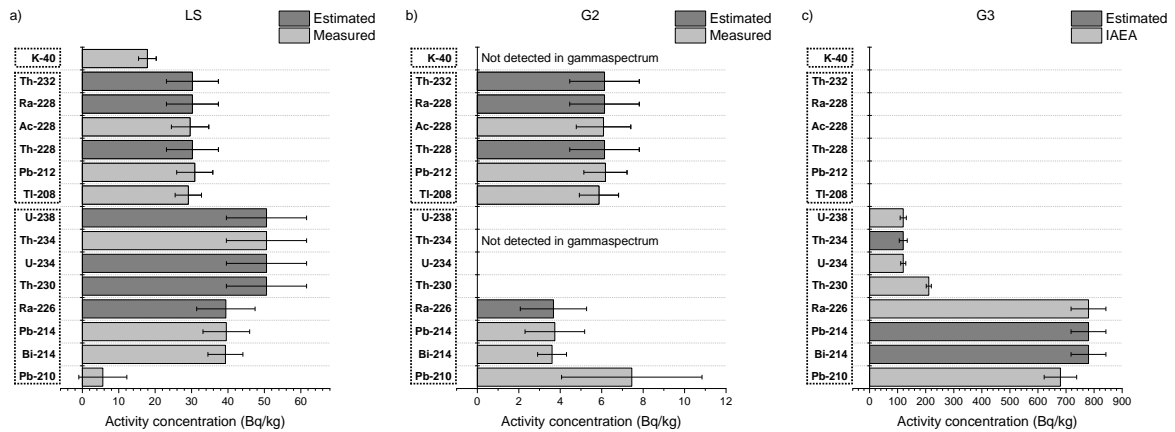
Figure 1: Activity concentrations (in Bq/kg, 2σ error) for a) LS, b) G2 and c) G3

The Ra_{eq} and the ACI were calculated with Eq. 1 and Eq. 2, respectively, for both paste and

mortar samples, and the results are presented in Fig. 2. It can be observed that the ACI is

stricter compared to the Ra_{eq}. For all samples, the calculated mean Ra_{eq} and ACI were

below the reference levels of 370 Bq/kg and 1, respectively, meaning that both paste and

mortar samples can directly be used as building material without radiological constraints.

Taking into account the 2σ error, the ACI for M6 (as a paste) was 0.98 ± 0.11 and

consequently exceeded slightly the reference level of 1. It has to be emphasized once more

that these indexes only serve as a conservative screening tool. Because pastes and mortars

are not directly used as a structural part of a building, it is more straightforward (and legally

relevant) to evaluate the ACI of concrete. Besides, aggregates used in concrete production

can also possess NOR. This could either increase or dilute the total NOR content, which has

to be evaluated for each specific case. Also the possible heterogeneity of industrial by-

products needs to be taken into account. The databases on NORM in construction materials

developed as part of the European COST Action TU1301 'NORM4BUILDING' [54] are a

valuable aid here.
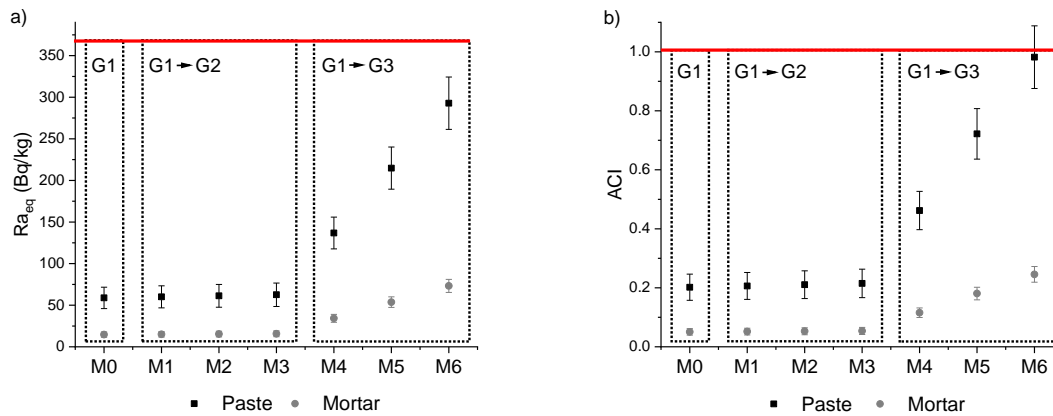
Figure 2: a) Ra_{eq} and b) ACI calculated for paste and mortar samples

3.2 Radon exhalation and emanation

The Ex_{Rn} and Em_{Rn} of mortar samples after 28 days of curing, calculated with Eq. 3 and Eq. 4, respectively, are shown in Fig. 3. The [226]Ra activity concentration of G2 was already very low (3.7 ± 1.6 Bq/kg) and consequently the substitution of G1 by G2 does not amend the overall [226]Ra activity concentration. Therefore, the Ex_{Rn} and Em_{Rn} of samples M0, M1, M2 and M3 are in the same order of magnitude (roughly around 30 mBq/(kg*h) and 50%, respectively). Compared to literature on mortars from standard cement (0.1 to 2.3 mBq/(kg*h) and 5 to 42% [47,55–58]) and mortars from (alkali-activated) NORM streams (6 to 12 mBq/(kg*h) [27,59] and 2 to 3.7% [55,59]) characterized by [226]Ra activity concentrations of the same range and approximately the same density, these values are slightly higher. Upon substituting G1 by G3, the [226]Ra activity concentration of samples M4, M5 and M6 gradually increases. Consequently the Ex_{Rn} becomes slightly higher, i.e., 88.5 ± 4.5 mBq/(kg*h), 78.8 ± 3.5 mBq/(kg*h) and 98.3 ± 2.8 mBq/(kg*h) for M4, M5 and M6, respectively. By contrast, the Em_{Rn} was the lowest among all samples, with values ranging from 36.8 ± 3.8% to 16.5 ± 0.9%. The Em_{Rn} is of particular interest because it indicates how large the fraction of the total [222]Rn generated is free to leave the building material, for which M6 was the best performing sample in this study. Assuming that the [226]Ra atoms are

15

332   homogeneously distributed throughout the samples and supposing an equal density, Em_{Rn} is

333   determined particularly by the microporosity [46,60,61]. This is consistent with Fig. 9 (see

334   further in section 3.5), where it is observed that both the volume and specific surface area of

335   the micropores decreases when moving from M4 to M6. At the same time, the mesoporosity

336   increases from M4 to M6 and consequently does not appear decisive regarding Em_{Rn}.
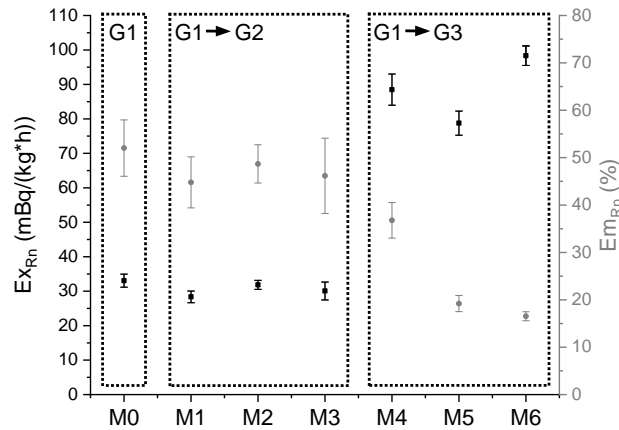
337

338   **Figure 3**: Ex_{Rn} and Em_{Rn} of mortar samples after 28 days of curing

339

340   **3.3 Microstructural analysis**

341   The microstructural analysis revealed the presence of ettringite (AFt), monosulfate (AFm),

342   aluminium-hydroxide (AH_3), and an amorphous calcium-(alumino)-silicate-hydrate gel (C-(A)-

343   S-H) as hydration products, which are indicated in Fig. 4a and Fig. 4b.
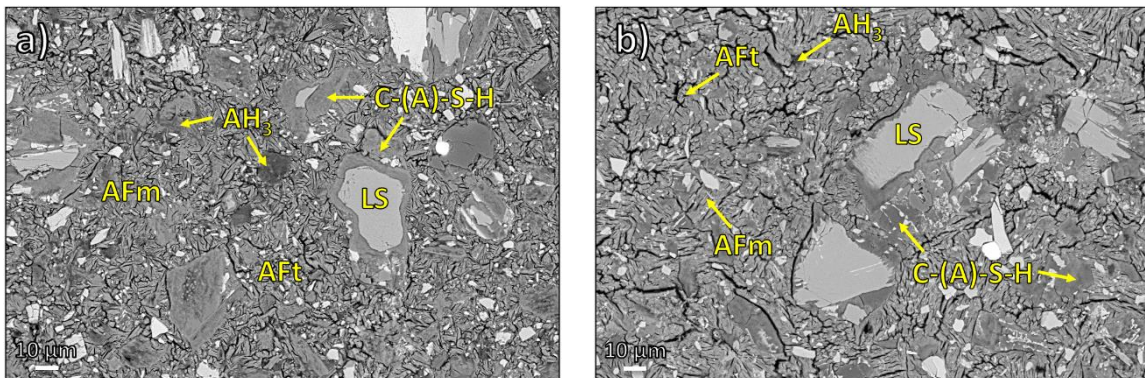
344

345   **Figure 4**: BSE image of a) M0 (paste, LS and G1) and b) M6 (paste, LS and G3)

346   The atomic ratios Al/Ca versus Si/Ca and Ca/Al versus S/Al, obtained from EDS (spots were

347   randomly distributed), are presented in Fig. 5. From Fig. 5a, it can be seen that there was a

348   relatively high level of intimate mixing of C-(A)-S-H with other hydration products [62],

349   evidenced by the cloud of data points. The C-(A)-S-H phase is characterized by a low Si/Ca

350   atomic ratio, which is in line with the low reactivity of $\gamma-C_2S$ [63,64]. It is worth mentioning

351   that, based on thermodynamic modelling of the pastes, strätlingite is thermodynamically

352   favorable in the system [65,66]. Hence, the C-(A)-S-H phase may convert to strätlingite after

353   extended curing periods. Fig. 5b plots the chemical composition of ettringite (AFt),

354   monosulfate (AFm, likely including its solid solutions), and aluminium-hydroxide (AH$_3$).

355   Monocarbonate was found in neither of the pastes. When gypsum gets substituted by PG

356   (i.e., the substitution of G1 by G3) (the green dots), the data move towards the binary

357   composition of aluminium-hydroxide (AH$_3$) and ettringite (AFt). By contrast, the use of G1

358   (the black dots) gave rise to the formation of monosulfate (AFm). Additional information

359   about the phase assemblage and their characterization is presented in [34]. The role of those

360   hydration products in leaching performance is elucidated in section 3.4.
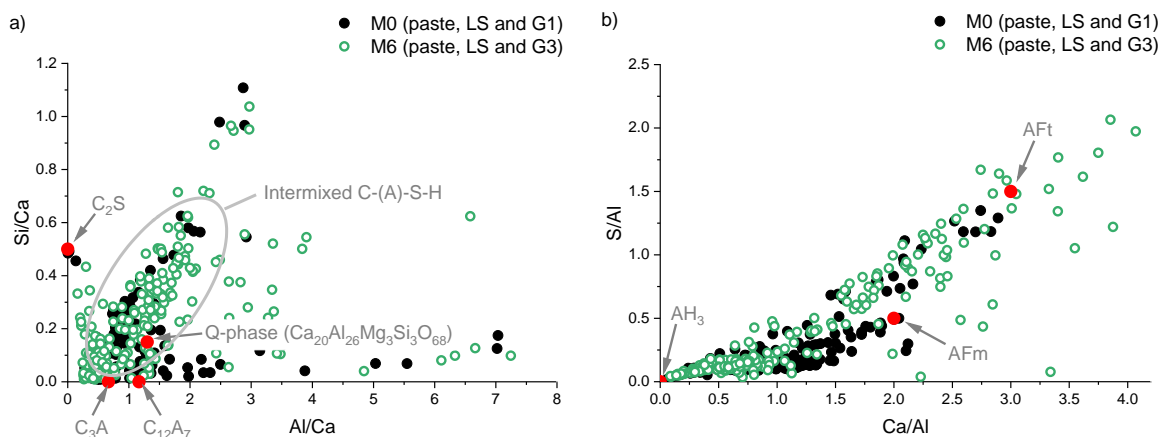
361

362   **Figure 5**: Atomic ratios obtained from EDS for a) Al/Ca versus Si/Ca and b) Ca/Al versus

363   S/Al (red dots represent the theoretical atomic ratios of the phases indicated)

364

3.4 Leaching assessment

The leaching of inorganic elements from the granulated mortars was assessed by an up-flow

percolation column test according to CEN/TS 16637-3 [33]. Fig. 6 shows the pH of the eluate

fractions, which was measured immediately after collection. The substitution of G1 by G2 did

not influence the eluate pH (Fig. 6a), while substitution by G3 resulted in a slightly lower

eluate pH (Fig. 6b). The stability domain for ettringite lies generally in the range from 10.5 to

13.0 [67], while the calcium-silicate-hydrate phase (C-S-H) starts to dissolve at a pH of

around 11 [68].
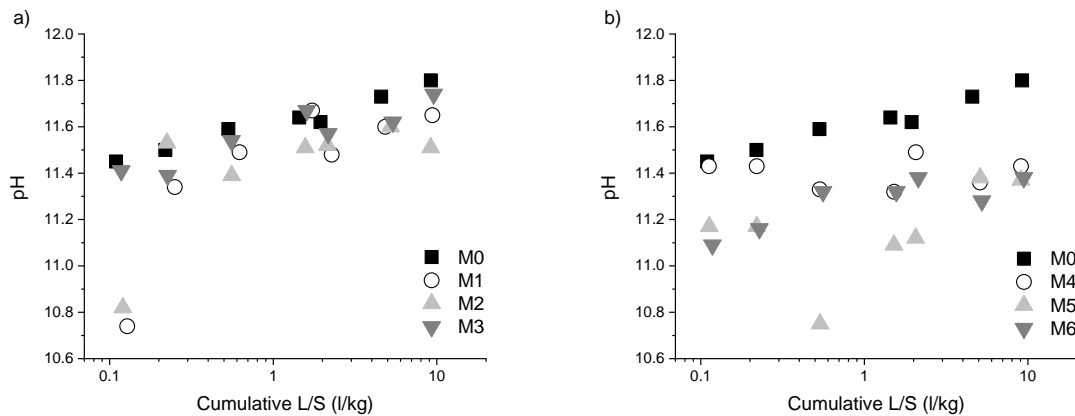
Figure 6: Eluate pH as a function of cumulative L/S upon substituting G1 by a) G2 and b) G3

Fig. 7 shows the concentrations of Al, Ca, F, Fe, Mg, S, Si and Sr in the eluates. The

concentrations of Ce, Mn, P and Ti were below the detection limit (0.01 mg/l, 0.01 mg/l, 0.10

mg/l and 0.05 mg/l, respectively) in each case. For Al and Ca, the quantities present in the

eluates ranged from 25 to 150 mg/l and from 70 to 160 mg/l, respectively. For the other

elements (i.e., F, Fe, Mg, S, Si and Sr), the concentrations were generally much lower, not

exceeding 22 mg/l. F was only present in G3 and therefore only measured for M4, M5 and

M6. For each element, except for Fe, the concentrations were variable during the experiment

and generally decreased when the L/S was increased. An increasing S concentration in the

eluates would indicate the decomposition of ettringite, which is not the case in this study.

From these patterns, the release mechanism for each individual element can be determined,

385   as described in CEN/TS 16637-3 [33]. The latter is useful in order to predict the long term

386   release during in-use and end-of-life situations of the material. The following release

387   mechanisms were identified: apparent depletion for Al and Sr; solubility controlled release for

388   Ca; and depletion for Mg. The overall release mechanisms for F, Fe, S and Si were variable
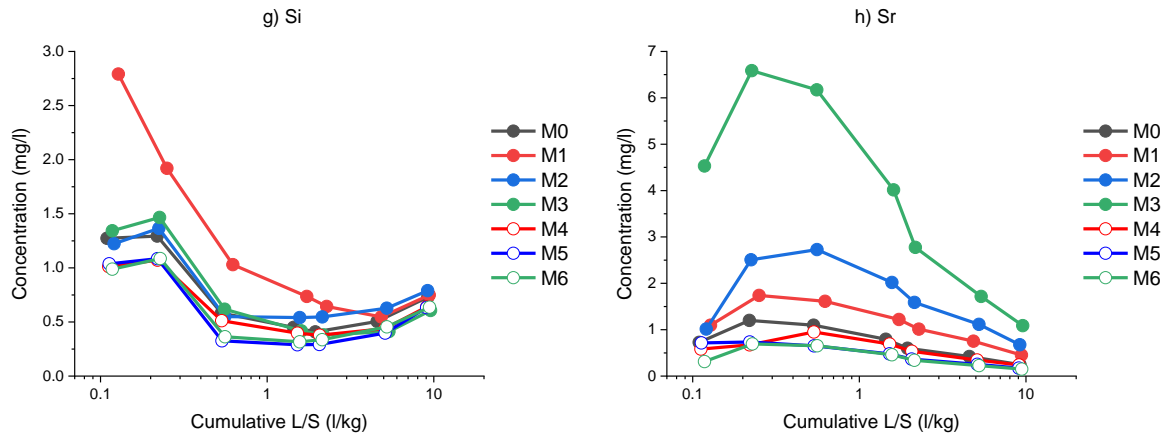
389   and remained unidentified.

390

391

392

393
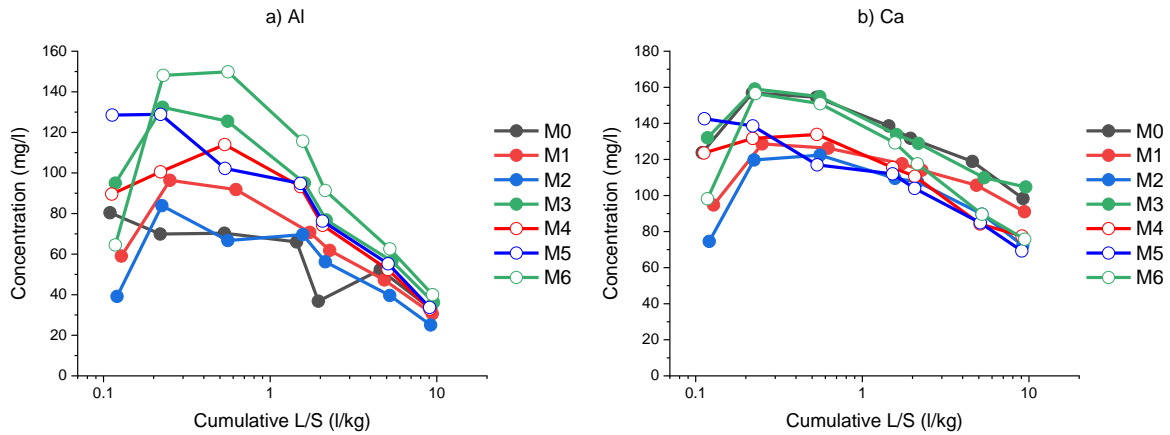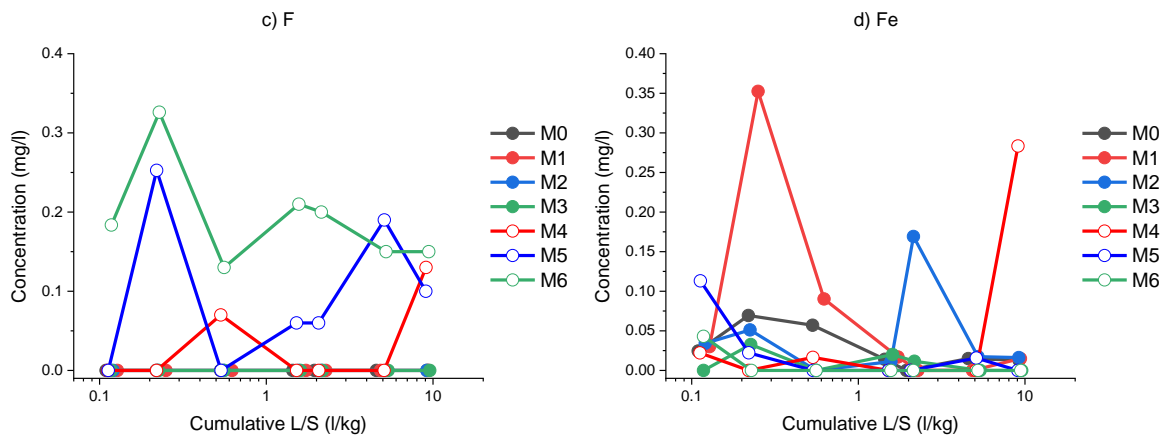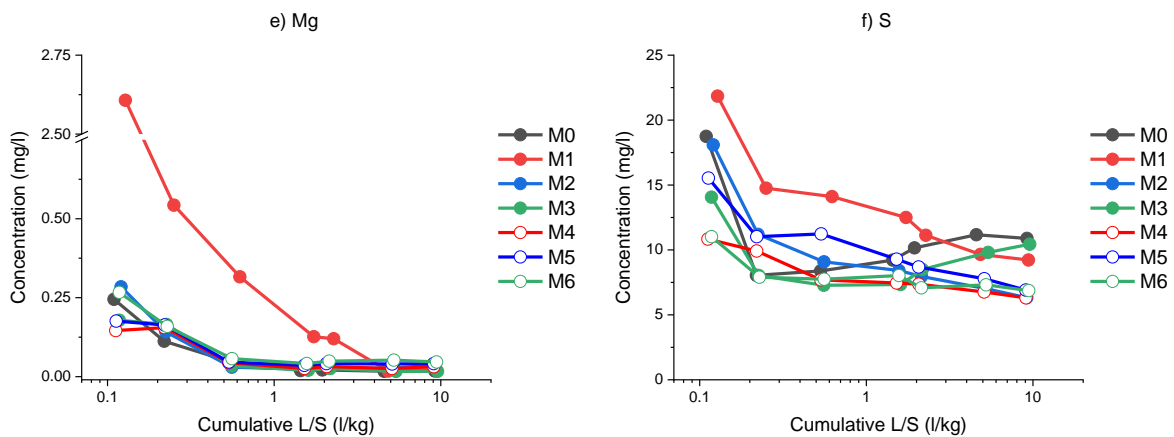
Figure 7: Concentrations as a function of cumulative L/S for a) Al, b) Ca, c) F, d) Fe, e) Mg,

f) S, g) Si and h) Sr

396 From the cumulative release (in mg/kg) at an L/S of 10.0 ± 0.5 l/kg (calculated from the data

397 in Fig. 7) and the elemental concentration of the samples (in mg/kg) (calculated from the data

398 in Table 1), the relative release was calculated and is shown in Fig. 8.

399 Immobilization of contaminants occurs by either physical or chemical processes or by a

400 combination thereof, as well as by the transport of dissolved ions to the eluate solution [69].

401 In case of retention by chemical means, the contaminant becomes part of the hydration

402 products by cation or oxyanion substitution. The ettringite structure can incorporate a number

403 of different ions, which is enviable for immobilization [30,70–72]. Trivalent ions can substitute

404 Al^{3+} in the ettringite structure [71], while bivalent ions can replace Ca^{2+} [29]. An example is

405 Fe-substituted ettringite ($C_6(A,F)\bar{S}_3H_{32}$) [68]. At the same time, SO_3^- can be replaced by

406 metal oxyanions [72]. However, it is most likely that the dominant anion (SO_3^-) forms

407 ettringite, while the remaining oxyanions either form monosulfate or interact by another

408 mechanism (i.e., sorption or physical inclusion) [72]. It has to be noted here that detailed X-

409 ray diffraction data on the existence of ettringite and monosulfate phases are presented in a

410 parallel study on the same binder mixtures [34]. However, ettringite does not seem to be

411 more effective in the immobilization of oxyanions than monosulfate [72]. Since the leaching

412 behavior of S is comparable for all samples (see Fig. 7f), the competition degree between

413   SO_3^- and other oxyanions for exchange sites in the ettringite (or monosulfate) structure is

414   comparable and independent of the (phospho-)gypsum source used. Next to ettringite,

415   aluminium-hydroxide and an amorphous C-(A)-S-H are found to constitute an important part

416   of the hydration products (see section 3.3). Aluminium-hydroxide is not significant regarding

417   immobilization [72]. On the other hand, immobilization by the C-(A)-S-H structure is more

418   efficient for cations because (1) Ca^{2+} can be substituted by bivalent cations and (2) the

419   sorption capacity for anions decreases with increasing pH [73]. This emphasizes that

420   ettringite plays an important role in oxyanion immobilization. The formation of insoluble (hydr-

421   )oxides and their physical encapsulation cannot be excluded.

422   The degree of stabilization for Ce, Mn, P and Ti is equal or nearly equal to 100% for all

423   samples, as their concentrations in the eluates were below the detection limit. At alkaline pH,

424   Ce is expected to precipitate as insoluble CeO_2 or $Ce(OH)_3$. However, Ce^{3+} could also be

425   incorporated into the ettringite and/or C-(A)-S-H structure. The same scenario is expected for

426   Mn, which can precipitate as Mn_3O_4 or $Mn(OH)_2$, or get incorporated as Mn^{2+} or Mn^{3+} in the

427   ettringite and/or C-(A)-S-H phase. P is likely incorporated in the ettringite structure as HPO_4^{2-}.

428   Ti transforms to anatase (TiO_2) in alkaline media or could be incorporated as Ti^{2+} or Ti^{3+} in

429   the hydration products. The relative release of F was comparable for mortars incorporated

430   with Polish PG (M4, M5 and M6) and ranged from 0.19 to 0.20%. In alkaline cementitious

431   matrices, F precipitates as insoluble CaF_2 [74,75]. However, F could also get incorporated in

432   the ettringite structure at the SO_4^{2-} site, or in other mineral phases (such as fluorellestadite)

433   [76,77]. The immobilization of Fe occurred most likely by the formation of Fe-substituted

434   ettringite. Fe release was highest for M4 (0.2%) and lowest for M6 (9.2×10^{-4} %), while M0

435   showed a release of 0.2×10^{-1} %. Mg release was very low and ranged from 0.5×10^{-2} to 0.2

436    $\times 10^{-1}$ %. Consequently, the immobilization degree exceeded 99.9% for all samples. Since

437   both Mg and Sr belong to the group of alkaline earth metals, they behave similarly to Ca and

438   can be incorporated in both the ettringite and C-(A)-S-H phase as Mg^{2+} and Sr^{2+}. Mortars

439   incorporated with Finnish PG (M1, M2 and M3) exhibit better fixation of Sr than those from

440   G1 (M0) and Polish PG (M4, M5 and M6). However, the degree of stabilization is over 90%

441   in each case. Sr release increases upon substitution of G1 by G2, while the reverse is seen

442   upon substitution of G1 by G3. The relative release for M0 was highest and amounted to

443   8.4%. For the more prominent elements (Al, Ca, S and Si) the relative release was

444   comparable for all samples (1.8 - 2.9%, 1 - 1.4%, 0.5 - 0.7% and 0.04 - 0.06%, respectively),

445   indicating that the same hydration products at comparable levels and stability were formed in

446   all samples, irrespective of the (phospho-)gypsum source used. According to the European

447   Drinking Water Directive [78], the Al and Fe concentration of (part of) the eluates exceeded

448   the parametric value (0.2 mg/l and 0.2 mg/l, respectively). Nevertheless, the pH for drinking

449   water purposes should be equal to or lower than 9.5 [78].
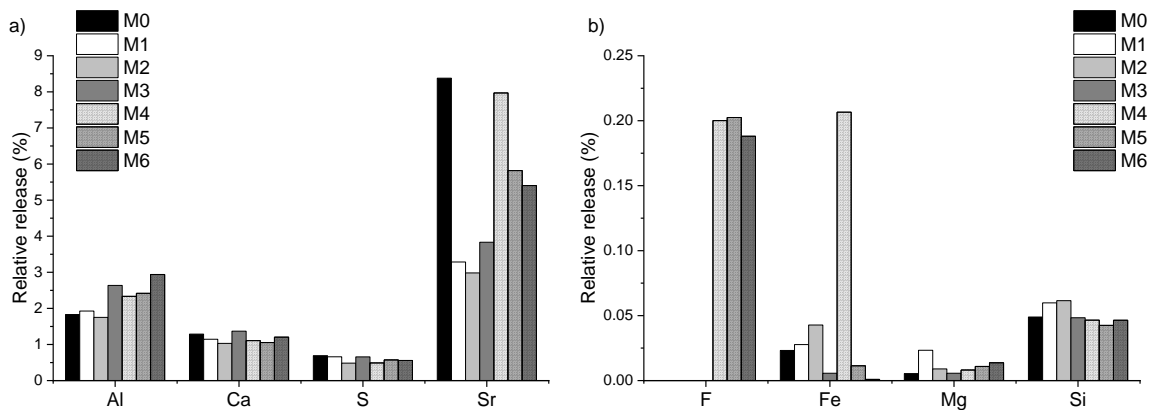
450

451   **Figure 8**: Relative release of a) Al, Ca, S, Sr and b) F, Fe, Mg, Si

452   The stability of the ettringite structure (both pH and temperature dependent) plays an

453   important role in unceasing immobilization. The conversion of ettringite to monosulfate is not

454   expected to be disastrous, as the monosulfate phase shows comparable or even better

455   immobilization potential [72]. However, when monosulfate converts again to ettringite at later

456   ages (delayed ettringite formation, DEF), catastrophic expansion occurs, potentially leading

457   to high release rates, failed immobilization and even environmental pollution. Because, in

458   real-life, multiple factors are simultaneously acting on building/construction materials (such

459   as (acid) rainfall, frost, growth of bacteria and fungi, carbonation, contact with seawater or

460 agricultural polluted waters, sulfate bearing groundwater, among others), possessing

461 synergistic and/or catalytic effects, extrapolation of lab-scale leaching tests to in-use and

462 end-of-life situations should be done with caution. For this reason, geochemical modeling

463 and an Eh-pH dependent leaching test could be interesting follow-up studies. The latter

464 would also provide confirmation on the preferential immobilization mechanism for each

465 element, since first the C-S-H phase will dissolve at a pH around 11, while ettringite remains

466 stable until a pH of around 10.5. However, one should keep in mind that the pH boundaries

467 of contaminant-substituted-ettringite (such as Fe-substituted-ettringite) can vary [72] and

468 should be carefully sought in order to avoid the generation of misleading results.

469

470 **3.5 Nitrogen adsorption/desorption**

471 The specific surface area and volume of the micro- and mesopores were assessed by means

472 of nitrogen adsorption/desorption and presented in Fig. 9. Upon the substitution of G1 by G2,

473 the specific surface area of the micropores increased, while the specific surface area of the

474 mesopores decreased. An opposite trend was observed when substituting G1 by G3, where

475 the specific surface area of the micropores decreased and the specific surface area of

476 mesopores increased. The same evolution is seen for the pore volume, with the lowest

477 micro- and mesopore volume obtained for M3. As already mentioned, the microporosity plays

478 a decisive role for radon release. Regarding leaching, it is not straightforward to compare the

479 results from Fig. 9 with leaching data, as the macroporosity should also be included. Despite

480 this, a low porosity is desirable in order to decrease the effects of carbonation among other

481 external factors, which could be detrimental for the stability of the hydration products

482 responsible for contaminant immobilization. Conventional cement shows generally specific

483 surface areas (obtained with nitrogen adsorption/desorption) in the range of 50 m²/g [79],

484 which is 20-30 times higher than the current mortars.
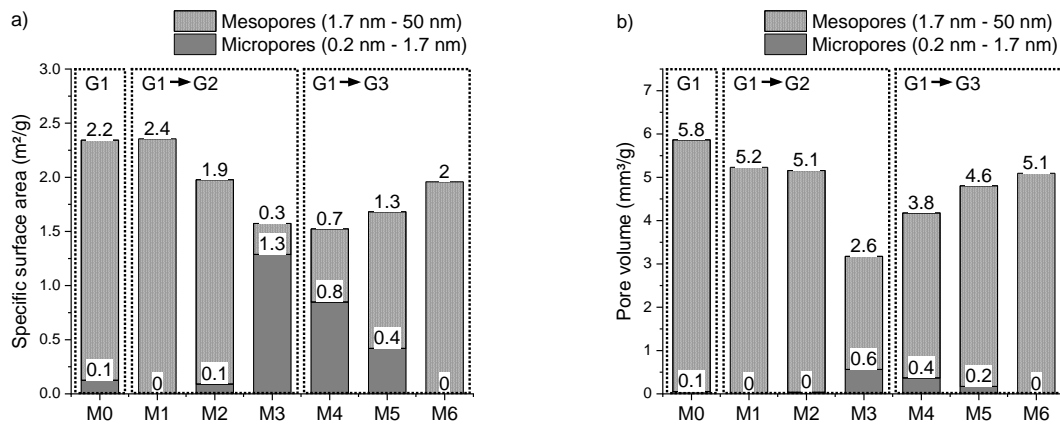
Figure 9: a) Specific surface area and b) pore volume

4. Conclusions

In this study, ettringite-based mortars were produced from LS and PG. Mortars were

incorporated with PGs of different origin in variable ratios and were compared with a

reference mortar from LS and synthetic gypsum. The used materials showed a variable

radionuclide content, which is a consequence of the terrestrial radionuclides from natural

origin present in the mineral ore that has been processed. Disequilibrium in the decay chains

results from their particular industrial processing. The Ra_{eq} and the ACI were calculated for

both paste and mortar samples allowing a conservative screening of the gamma dose rate.

In each case, the obtained mean values were below the legal reference levels, indicating that

the produced mortars can safely be used for building purposes. The radon emanation

decreased upon increasing the Polish PG content. For those mortars, the emanation was

mainly determined by the microporosity, while the mesoporosity appeared to be not decisive.

The mortars were found to exhibit extremely low micro- and mesoporosity, with specific

surface areas between 20-30 times lower than conventional cement (1.5-2.5 m²/g). The

immobilization degree for contaminants such as Ce, Mn, P and Ti from PG was equal or

nearly equal to 100% for all samples, while retention of F, Fe and Mg exceeded 99% and

stabilization of Sr was over 90%. However, extrapolation of lab-scale leaching tests to in-use

505 and end-of-life situations should be done with caution. This investigation shows high potential

506 for PG reuse in ettringite-based mortars.

507

508 **Declarations of interest:** none

509

510 **Acknowledgements**

517

518 **References**

519 [1] C. Shi, A.F. Jiménez, A. Palomo, New cements for the 21st century: The pursuit of an
520 alternative to Portland cement, Cem. Concr. Res. 41 (2011) 750–763.
521 doi:10.1016/j.cemconres.2011.03.016.

522 [2] H. Motz, J. Geiseler, Products of steel slags an opportunity to save natural resources,
523 Waste Manag. 21 (2001) 285–293. doi:10.1016/S0956-053X(00)00102-1.

524 [3] D.W. Lewis, Properties and uses of iron and steel slags, National Slag Association,
525 1982. http://www.nationalslag.org/sites/nationalslag/files/documents/nsa_182-
526 6_properties_and_uses_slag.pdf.

527 [4] J.M. Manso, M. Losanez, J.A. Polanco, J.J. Gonzalez, Ladle furnace slag in
528 construction, J. Mater. Civ. Eng. 17 (2005) 513–518. doi:10.1061/(ASCE)0899-
529 1561(2005)17:5(513).

530 [5] V.Z. Serjun, B. Mirtič, A. Mladenovič, Evaluation of ladle slag as a potential material
531 for building and civil engineering, Mater. Tehnol. 47 (2013) 543–550.

532 [6] E. Adesanya, K. Ohenoja, P. Kinnunen, M. Illikainen, Alkali activation of ladle slag
533 from steel-making process, J. Sustain. Metall. 3 (2017) 300–310. doi:10.1007/s40831-
534 016-0089-x.

535 [7] E. Adesanya, K. Ohenoja, P. Kinnunen, M. Illikainen, Properties and durability of
536 alkali-activated ladle slag, Mater. Struct. Constr. 50 (2017) 1–10. doi:10.1617/s11527-

537   017-1125-4.

538 [8] H. Nguyen, V. Carvelli, E. Adesanya, P. Kinnunen, M. Illikainen, High performance
539   cementitious composite from alkali-activated ladle slag reinforced with polypropylene
540   fibers, Cem. Concr. Compos. 90 (2018) 150–160.
541   doi:10.1016/j.cemconcomp.2018.03.024.

542 [9] H. Nguyen, P. Kinnunen, V. Carvelli, M. Mastali, M. Illikainen, Strain hardening
543   polypropylene fiber reinforced composite from hydrated ladle slag and gypsum,
544   Compos. Part B Eng. 158 (2019) 328–338. doi:10.1016/j.compositesb.2018.09.056.

545 [10] S. Rubert, C.A. Luz, M.V.F. Varela, J.I.P. Filho, R.D. Hooton, Hydration mechanisms
546   of supersulfated cement: The role of alkali activator and calcium sulfate content, J.
547   Therm. Anal. Calorim. 134 (2018) 971–980. doi:10.1007/s10973-018-7243-6.

548 [11] A. Gruskovnjak, B. Lothenbach, F. Winnefeld, R. Figi, S.C. Ko, M. Adler, U. Mäder,
549   Hydration mechanisms of super sulphated slag cement, Cem. Concr. Res. 38 (2008)
550   983–992. doi:10.1016/j.cemconres.2008.03.004.

551 [12] E.G. Moffatt, M.D.A. Thomas, Durability of rapid-strength concrete produced with
552   ettringite-based binders, ACI Mater. J. 115 (2018). doi:10.14359/51701006.

553 [13] B.C. McLellan, R.P. Williams, J. Lay, A. Van Riessen, G.D. Corder, Costs and carbon
554   emissions for geopolymer pastes in comparison to ordinary portland cement, J. Clean.
555   Prod. 19 (2011) 1080–1090. doi:10.1016/j.jclepro.2011.02.010.

556 [14] S. Suarez, X. Roca, S. Gasso, Product-specific life cycle assessment of recycled
557   gypsum as a replacement for natural gypsum in ordinary Portland cement: Application
558   to the Spanish context, J. Clean. Prod. 117 (2016) 150–159.
559   doi:10.1016/j.jclepro.2016.01.044.

560 [15] International Atomic Energy Agency (IAEA), Management of NORM Residues, IAEA-
561   TECDOC-1712, Vienna, 2013.

562 [16] H. Tayibi, M. Choura, F.A. López, F.J. Alguacil, A. López-Delgado, Environmental
563   impact and management of phosphogypsum, J. Environ. Manage. 90 (2009) 2377–
564   2386. doi:10.1016/j.jenvman.2009.03.007.

565 [17] International Atomic Energy Agency (IAEA), Radiation Protection and Management of
566   NORM Residues in the Phosphate Industry, Safety Reports Series No. 78, IAEA,
567   Vienna, 2013. doi:10.1016/j.resourpol.2012.04.002.

568 [18] United Nations Scientific Committee on the Effects of Atomic Radiation (UNSCEAR),
569   Sources and Effects of Ionizing Radiation: UNSCEAR 2008 Report to the General
570   Assembly with Scientific Annexes, New York, 2010.

571 [19] World Health Organization (WHO), Who Handbook on Indoor Radon - A Public Health
572   Perspective, first ed., WHO, Geneva, 2009. doi:10.1080/00207230903556771.

573 [20] K. Kovler, Radiological constraints of using building materials and industrial by-
574   products in construction, Constr. Build. Mater. 23 (2009) 246–253.
575   doi:10.1016/j.conbuildmat.2007.12.010.

576 [21] C. Nuccetelli, Y. Pontikes, F. Leonardi, R. Trevisi, New perspectives and issues
577   arising from the introduction of (NORM) residues in building materials: A critical
578   assessment on the radiological behaviour, Constr. Build. Mater. 82 (2015) 323–331.
579   doi:10.1016/j.conbuildmat.2015.01.069.

580 [22] J. Beretka, P.J. Matthew, Natural radioactivity of Australian building materials,
581   industrial wastes and by products, Health Phys. 48 (1985) 87–95.
582   doi:10.1097/00004032-198501000-00007.

[23] C. Nuccetelli, G. de With, R. Trevisi, N. Vanhoudt, S. Pepin, H. Friedmann, G. Xhixha, W. Schroeyers, J. Aguiar, J. Hondros, B. Michalik, K. Kovler, A. Janssens, R. Wiegers, Legislative aspects, in: Nat. Occur. Radioact. Mater. Constr., Woodhead Publishing, 2017: pp. 37–60. doi:10.1016/B978-0-08-102009-8.00004-9.

[24] Council of the European Union, Council directive 2013/59/EURATOM, European Basic Safety Standards (BSS) for Protection against Ionising Radiation, Off. J. Eur. Union. L 13/1 (2014).

[25] International Agency for Research on Cancer (IARC), IARC monographs on the identification of carcinogenic hazards to humans, List Classif. Agents Classif. by IARC Monogr. Vol. 1-124. (2019). https://monographs.iarc.fr/list-of-classifications.

[26] Y. Ishimori, K. Lange, P. Martin, Y.S. Mayya, M. Phaneuf, Technical Reports Series No. 474: Measurement and Calculation of Radon Releases from NORM Residues, Vienna, 2013.

[27] K. Gijbels, R. Ion Iacobescu, Y. Pontikes, N. Vandevenne, S. Schreurs, W. Schroeyers, Radon immobilization potential of alkali-activated materials containing ground granulated blast furnace slag and phosphogypsum, Constr. Build. Mater. 184 (2018) 68–75. doi:10.1016/j.conbuildmat.2018.06.162.

[28] Q. Zhou, N.B. Milestone, M. Hayes, An alternative to Portland Cement for waste encapsulation-The calcium sulfoaluminate cement system, J. Hazard. Mater. 136 (2006) 120–129. doi:10.1016/j.jhazmat.2005.11.038.

[29] M.L.D. Gougar, B.E. Scheetz, D.M. Roy, Ettringite and C-S-H portland cement phases for waste ion immobilization: A review, Waste Manag. 16 (1996) 295–303. doi:10.1016/S0956-053X(96)00072-4.

[30] V. Albino, R. Cioffi, M. Marroccoli, L. Santoro, Potential application of ettringite generating systems for hazardous waste stabilization, J. Hazard. Mater. 51 (1996) 241–252. doi:10.1016/S0304-3894(96)01828-6.

[31] O. Hjelmar, M. Wahlström, R. Comans, U. Kalbe, P. Grathwohl, J. Mehu, N. Schiopu, J. Hykš, J. Laine-ylijoki, A. van Zomeren, O. Krüger, U. Schoknecht, T. Wendel, M. Abdelghafour, N. Borho, Robustness validation of two harmonized European leaching tests for assessment of the leaching of construction products, including waste-based construction materials, in: WASCON 2012 Gothenburg, Sweden, 2012: pp. 1–5.

[32] European Committee for Standardization, CEN/TC 351. Construction Products: Assessment of release of dangerous substances, (2014).

[33] European Committee for Standardization, CEN/TS 16637-3. Construction products: Assessment of release of dangerous substances - Part 3: Horizontal up-flow percolation test, (2016).

[34] K. Gijbels, H. Nguyen, P. Kinnunen, W. Schroeyers, Y. Pontikes, S. Schreurs, M. Illikainen, Feasibility of incorporating phosphogypsum in ettringite-based binder from ladle slag, J. Clean. Prod. 237 (2019) 117793. doi:10.1016/j.jclepro.2019.117793.

[35] European Committee for Standardization, EN 450-1: Fly ash for concrete - Part 1: Definition, specifications and conformity criteria, (2012).

[36] A. Shakhashiro, U. Sansone, H. Wershofen, A. Bollhöfer, C.K. Kim, C.S. Kim, G. Kis-Benedek, M. Korun, M. Moune, S.H. Lee, S. Tarjan, M.S. Al-Masri, The new IAEA reference material: IAEA-434 technologically enhanced naturally occurring radioactive materials (TENORM) in phosphogypsum, Appl. Radiat. Isot. 69 (2011) 231–236. doi:10.1016/j.apradiso.2010.09.002.

[37] L. Lutterotti, S. Matthies, H.R. Wenk, MAUD (Material Analysis Using Diffraction): a

630 user friendly java program for Rietveld texture analysis and more, in: Jerzy A. Szpunar
631 (Ed.), Proc. Twelfth Int. Conf. Textures Mater. / ICOTOM-12, National Research
632 Press, Montreal, 1999: p. 1599.

633 [38] H.M. Rietveld, A profile refinement method for nuclear and magnetic structures, J.
634 Appl. Crystallogr. 2 (1969) 65–71. doi:10.1107/S0021889869006558.

635 [39] B. Michalik, G. de With, W. Schroeyers, Measurement of radioactivity in building
636 materials - Problems encountered caused by possible disequilibrium in natural decay
637 series, Constr. Build. Mater. 168 (2018) 995–1002.
638 doi:10.1016/j.conbuildmat.2018.02.044.

639 [40] Laboratoire National Henri Becquerel (LNHB), Decay Data Evaluation Project, (n.d.).
640 http://www.nucleide.org/DDEP.htm.

641 [41] European Committee for Standardization, EN 196-6. Methods of testing cement - Part
642 6: Determination of fineness, (2010).

643 [42] OECD (Organization for Economic Cooperation and Development), Exposure to
644 radiation from the natural radioactivity in building materials, Paris, 1979.

645 [43] J. Somlai, B. Kanyár, R. Bodnár, C. Németh, Z. Lendvai, Radiation dose contribution
646 from coal-slags used as structural building material, J. Radioanal. Nucl. Chem. Artic.
647 207 (1996) 437–443. doi:10.1007/BF02071248.

648 [44] C. Nuccetelli, F. Leonardi, R. Trevisi, A new accurate and flexible index to assess the
649 contribution of building materials to indoor gamma exposure, J. Environ. Radioact. 143
650 (2015) 70–75. doi:10.1016/j.jenvrad.2015.02.011.

651 [45] T. Croymans, F. Leonardi, R. Trevisi, C. Nuccetelli, S. Schreurs, W. Schroeyers,
652 Gamma exposure from building materials - A dose model with expanded gamma lines
653 from naturally occurring radionuclides applicable in non-standard rooms, Constr. Build.
654 Mater. 159 (2017) 768–778. doi:10.1016/j.conbuildmat.2017.10.051.

655 [46] Z. Sas, J. Szántó, J. Kovács, J. Somlai, T. Kovács, Influencing effect of heat-treatment
656 on radon emanation and exhalation characteristic of red mud, J. Environ. Radioact.
657 148 (2015) 27–32. doi:10.1016/J.JENVRAD.2015.06.002.

658 [47] K. Kovler, A. Perevalov, V. Steiner, L.A. Metzger, Radon exhalation of cementitious
659 materials made with coal fly ash: Part 1 - Scientific background and testing of the
660 cement and fly ash emanation, J. Environ. Radioact. 82 (2005) 321–334.
661 doi:10.1016/j.jenvrad.2005.02.004.

662 [48] K. Gijbels, S. Landsberger, P. Samyn, R. Ion Iacobescu, Y. Pontikes, S. Schreurs, W.
663 Schroeyers, Radiological and non-radiological leaching assessment of alkali-activated
664 materials containing ground granulated blast furnace slag and phosphogypsum, Sci.
665 Total Environ. 660 (2019) 1098–1107. doi:10.1016/j.scitotenv.2019.01.089.

666 [49] S. Brunauer, P.H. Emmett, E. Teller, Adsorption of gases in multimolecular layers, J.
667 Am. Chem. Soc. 60 (1938) 309–319. doi:10.1021/ja01269a023.

668 [50] E.P. Barrett, L.G. Joyner, P.P. Halenda, The determination of pore volume and area
669 distributions in porous substances. I. Computations from nitrogen isotherms, J. Am.
670 Ceram. Soc. 73 (1951) 373–380.

671 [51] B.C. Lippens, J.H. de Boer, Studies on pore systems in catalysts: V. The t method, J.
672 Catal. 4 (1965) 319–323. doi:10.1016/0021-9517(65)90307-6.

673 [52] European Commission, Radiological protection principles concerning the natural
674 radioactivity of building materials - Radiation Protection 112, Luxemburg, 1999.
675 https://ec.europa.eu/energy/sites/ener/files/documents/112.pdf.

676 [53] J.P. Bolivar, R. García-Tenorio, M. García-León, On the fractionation of natural
677 radioactivity in the production of phosphoric acid by the wet acid method, J. Radioanal.
678 Nucl. Chem. Lett. 214 (1996) 77–88. doi:10.1007/BF02164808.

679 [54] W. Schroeyers, Z. Sas, G. Bator, R. Trevisi, C. Nuccetelli, F. Leonardi, S. Schreurs, T.
680 Kovacs, The NORM4Building database, a tool for radiological assessment when using
681 by-products in building materials, Constr. Build. Mater. 159 (2018) 755–767.
682 doi:10.1016/j.conbuildmat.2017.11.037.

683 [55] S.C. Taylor-Lange, M.C.G. Juenger, J.A. Siegel, Radon emanation fractions from
684 concretes containing fly ash and metakaolin, Sci. Total Environ. 466–467 (2014)
685 1060–1065. doi:10.1016/j.scitotenv.2013.08.005.

686 [56] P. de Jong, W. van Dijk, The effect of the composition and production process of
687 concrete on the 222Rn exhalation rate, Environ. Int. 22 (1996) 287–293.
688 doi:10.1016/S0160-4120(96)00120-1.

689 [57] J.G. Ackers, J.F. Den Boer, P. De Jong, R.A. Wolschrijn, Radioactivity and radon
690 exhalation rates of building materials in The Netherlands, Sci. Total Environ. 45 (1985)
691 151–156. doi:10.1016/0048-9697(85)90215-3.

692 [58] K. Kovler, Does the utilization of coal fly ash in concrete construction present a
693 radiation hazard?, Constr. Build. Mater. 29 (2012) 158–166.
694 doi:10.1016/j.conbuildmat.2011.10.023.

695 [59] Z. Sas, W. Sha, M. Soutsos, R. Doherty, D. Bondar, K. Gijbels, W. Schroeyers,
696 Radiological characterisation of alkali-activated construction materials containing red
697 mud, fly ash and ground granulated blast-furnace slag, Sci. Total Environ. 659 (2019)
698 1496–1504. doi:10.1016/j.scitotenv.2019.01.006.

699 [60] W. Zhang, Y. Zhang, Q. Sun, Analyses of influencing factors for radon emanation and
700 exhalation in soil, Water. Air. Soil Pollut. 230 (2019). doi:10.1007/s11270-018-4063-z.

701 [61] K. Kovler, Mechanisms of radon exhalation from hardening cementitious materials,
702 ACI Mater. J. 105 (2008) 404–413.

703 [62] J.E. Rossen, K.L. Scrivener, Optimization of SEM-EDS to determine the C–A–S–H
704 composition in matured cement paste samples, Mater. Charact. 123 (2017) 294–306.
705 doi:10.1016/j.matchar.2016.11.041.

706 [63] D. Herfort, D.E. Macphee, Components in Portland cement clinker and their phase
707 relationships, in: P.C. Hewlett, M. Liska (Eds.), Lea's Chem. Cem. Concr., 5th ed.,
708 Butterworth-Heinemann, 2019: pp. 57–86. doi:10.1016/B978-0-08-100773-0.00003-4.

709 [64] L. Kriskova, Y. Pontikes, Ö. Cizer, G. Mertens, W. Veulemans, D. Geysen, P.T. Jones,
710 L. Vandewalle, K. Van Balen, B. Blanpain, Effect of mechanical activation on the
711 hydraulic properties of stainless steel slags, Cem. Concr. Res. 42 (2012) 778–788.
712 doi:10.1016/j.cemconres.2012.02.016.

713 [65] Y. Jeong, C.W. Hargis, S.C. Chun, J. Moon, The effect of water and gypsum content
714 on strätlingite formation in calcium sulfoaluminate-belite cement pastes, Constr. Build.
715 Mater. 166 (2018) 712–722. doi:10.1016/j.conbuildmat.2018.01.153.

716 [66] B. Lothenbach, D.A. Kulik, T. Matschei, M. Balonis, L. Baquerizo, B. Dilnesa, G.D.
717 Miron, R.J. Myers, Cemdata18: A chemical thermodynamic database for hydrated
718 Portland cements and alkali-activated materials, Cem. Concr. Res. 115 (2019) 472–
719 506. doi:10.1016/j.cemconres.2018.04.018.

720 [67] R.B. Perkins, C.D. Palmer, Solubility of ettringite (Ca6[Al(OH)6]2(SO4)326H2O) at 5–
721 75°C, Geochim. Cosmochim. Acta. 63 (1999) 1969–1980. doi:10.1016/S0016-
722 7037(99)00078-2.

723   [68] W.A. Klemm, J.I. Bhatty, Fixation of heavy metals as oxyanion-substituted ettringites,
724   Skokie, Illinois, USA, 2002.

725   [69] I. Fernández-Olmo, C. Lasa, M.A. Lavín, A. Irabien, Modeling of amphoteric heavy
726   metals solubility in stabilized/solidified steel foundry dust, Environ. Eng. Sci. 26 (2008)
727   251–262. doi:10.1089/ees.2007.0226.

728   [70] S. Peysson, J. Péra, M. Chabannet, Immobilization of heavy metals by calcium
729   sulfoaluminate cement, Cem. Concr. Res. 35 (2005) 2261–2270.
730   doi:10.1016/j.cemconres.2005.03.015.

731   [71] R. Berardi, R. Cioffi, L. Santoro, Matrix stability and leaching behaviour in ettringite-
732   based stabilization systems doped with heavy metals, Waste Manag. 17 (1997) 535–
733   540. doi:10.1016/S0956-053X(97)10061-7.

734   [72] M. Chrysochoou, D. Dermatas, Evaluation of ettringite and hydrocalumite formation for
735   heavy metal immobilization: Literature review and experimental study, J. Hazard.
736   Mater. 136 (2006) 20–33. doi:10.1016/j.jhazmat.2005.11.008.

737   [73] H.A. Van der Sloot, Characterization of the leaching behaviour of concrete mortars
738   and of cement-stabilized wastes with different waste loading for long term
739   environmental assessment, Waste Manag. 22 (2002) 181–186. doi:10.1016/S0956-
740   053X(01)00067-8.

741   [74] B.I. Silveira, A.E.M. Dantas, J.E.M. Blasques, R.K.P. Santos, Effectiveness of cement-
742   based systems for stabilization and solidification of spent pot liner inorganic fraction, J.
743   Hazard. Mater. 98 (2003) 183–190. doi:10.1016/S0304-3894(02)00317-5.

744   [75] J.Y. Park, H.J. Byun, W.H. Choi, W.H. Kang, Cement paste column for simultaneous
745   removal of fluoride, phosphate, and nitrate in acidic wastewater, Chemosphere. 70
746   (2008) 1429–1437. doi:10.1016/j.chemosphere.2007.09.012.

747   [76] A.F.S. Gomes, D.L. Lopez, A.C.Q. Ladeira, Characterization and assessment of
748   chemical modifications of metal-bearing sludges arising from unsuitable disposal, J.
749   Hazard. Mater. 199–200 (2012) 418–425. doi:10.1016/j.jhazmat.2011.11.039.

750   [77] H. He, H. Suito, Immobilization of fluorine in aqueous solution by calcium aluminum
751   ferrite and the mixture of calcium aluminate and gypsum, ISIJ Int. 42 (2008) 794–799.
752   doi:10.2355/isijinternational.42.794.

753   [78] Council of the European Union, European drinking water directive
754   2013/51/EURATOM, laying down requirements for the protection of the health of the
755   general public with regard to radioactive substances in water intended for human
756   consumption, Off. J. Eur. Union. L 296/12 (2013). http://eur-lex.europa.eu/legal-
757   content/EN/TXT/?uri=CELEX%3A32013L0051.

758   [79] W. Kurdowski, Cement and concrete chemistry, Springer, Krakow, Poland, 2014.
759   doi:10.1007/978-94-007-7945-7.

760

761